



# Achieving high efficiency silicon heterojunction solar cells by applying high hydrogen content amorphous silicon as epitaxial-free buffer layers

Tianyu Ruan<sup>a</sup>, Minghao Qu<sup>b,\*</sup>, Xianlin Qu<sup>a</sup>, Xiaoning Ru<sup>b</sup>, Jianqiang Wang<sup>a</sup>, Yongcai He<sup>a</sup>, Kun Zheng<sup>a</sup>, Bo Heb Hongfeng Lin<sup>b</sup>, Xixiang Xu<sup>b</sup>, Yongzhe Zhang<sup>a,\*</sup>, Hui Yan<sup>a,\*</sup>

<sup>a</sup> College of Materials Science and Engineering, Key Laboratory of Advanced Functional Materials of Education Ministry of China, Beijing Key Laboratory of Microstructure and Properties of Solids, Beijing University of Technology, Beijing 100124, China

<sup>b</sup> Hanergy Thin Film Power Group Ltd., Chengdu R&D Center, Chengdu, Sichuan 610200, China



## ABSTRACT

High hydrogen content ( $C_H$ ) intrinsic amorphous silicon (a-Si:H) buffer layers were deposited on both sides of crystalline silicon wafers using plasma-enhanced chemical vapor deposition technique, which significantly improved surface passivation as well as conversion efficiency of the silicon heterojunction solar cells. Properties of the buffer layer and impact on the device performance were investigated. High resolution transmission electron microscope characterization shows that no obvious epitaxial growth occurred at the interface as long as a-Si:H buffer layer was introduced between c-Si and bulk intrinsic layer. Further study indicates that minority carrier lifetime of the device is related to hydrogen content of the buffer layer, reaching highest value up to 2050 ms at  $C_H$  of 33%. These findings evidently confirmed that suppression of epitaxial growth and thus improved passivation were realized by using high-hydrogen-content a-Si:H buffer layer, based on which a high efficiency solar cell was prepared with large area.

## 1. Introduction

In recent years, an increasing number of silicon solar cells with efficiencies more than 25% were reported [1-6]. Among the high efficiency silicon solar cells, silicon heterojunction (SHJ) solar cell has attracted a lot of attentions due to its high performance, reasonable production cost and low thermal budget [7, 8]. Silicon heterojunction with interdigitated back contacts (SHJ-IBC) solar cell on a wafer of large area ( $179.7 \text{ cm}^2$ ) has reached a record conversion efficiency up to 26.7%, which is approaching the theoretical limit of 29% of silicon based solar cells [1]. In order to realize high efficiency for SHJ solar cells, a well defect passivated c-Si surface by intrinsic amorphous silicon (i-a-Si:H) layer prior to deposition of the n/p-doped layers is critical, as the i-a-Si:H layer can significantly reduce the surface-defect-related recombination losses, resulting in high open circuit voltage ( $V_{oc}$ ) up to 750 mV [9-11]. However, it was found that epitaxial growth can be easily formed when i-a-Si:H layer was deposited by plasma enhanced chemical vapor deposition (PECVD). Interfacial layers such as very porous a-Si:H layers with high ( $\text{SiH}_2$ ), were introduced to prevent epitaxial growth at the interface [12, 13], as  $(\text{SiH}_2)_n$  represents loose and defective species in a-Si:H films, however leading to formation of defects in the films [14]. Thus, the a-Si:H deposition parameters are restrained in a narrow range, which limits optimization of the process conditions [15]. This trade-off between low defect a-Si:H film and

epitaxial growth at a-Si:H/c-Si interface makes it challenging to form a good passivation at the interface. In previous work, our group have reported that a two-step method for preparing the amorphous silicon passivation layers, good passivation quality can be obtained when the buffer layer thickness varies from 2 nm to 5 nm, showing great potential in industrialization [12]. Liu et al. have reported that underdense a-Si:H performs better than transition-zone a-Si:H for passivating the c-Si surfaces of SHJ solar cells [16]. However, there is limited literature that relates the interfacial structure to hydrogen content of buffer layer for applications in SHJ solar cell. Further improvement is required and can be achieved by controlling and optimizing the interfacial buffer layer.

In this study, we deposited a high  $C_H$  buffer layer ( $i_1$ ) with pure silane plasma, following by deposition of intrinsic bulk layer ( $i_2$ ) with a high  $H_2$  dilution. The  $i_1$  layer suppressed the epitaxial growth at interface effectively with acceptable film quality, while low-defect  $i_2$  bulk layer further promoted passivation quality. Detailed analyses such as Fourier transform infrared (FTIR), minority carrier lifetime and high-resolution transmission electron microscope (HR-TEM) were conducted to elucidate the relationships between device performance and process conditions of the  $i_1$  layer.

## 2. Experiments

In this study, SHJ solar cells were fabricated on n-type M2 semi

\* Corresponding authors.

E-mail addresses: [quminghao@hanergy.com](mailto:quminghao@hanergy.com) (M. Qu), [yzzhang@bjut.edu.cn](mailto:yzzhang@bjut.edu.cn) (Y. Zhang), [hyan@bjut.edu.cn](mailto:hyan@bjut.edu.cn) (H. Yan).

**Table 1**  
R and C<sub>H</sub> corresponding to the processing parameters.

Process conditions	w/o i <sub>1</sub> s(i <sub>2</sub> only)	A	B	C	D
Power density (mW/cm <sup>2</sup> )	15	15	30	45	60
Pressure (Pa)	50	40	50	70	90
Deposition rate (Å/s)	1.11	2.57	6.77	10.1	14.9
Microstructure factor R (%)	4.54	8.97	47.6	60.4	74.8
Hydrogen content C <sub>H</sub> (%)	14.95	18.0	25.9	33.3	35.9

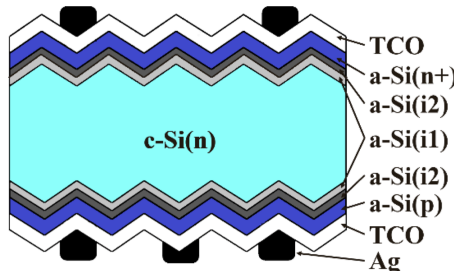


Fig. 1. Cross-sectional view of the SHJ solar cells.

square Czochralski (CZ) (100) c-Si wafers ( $156.75 \times 156.75 \text{ mm}^2$ ) of  $\sim 180 \mu\text{m}$  thickness and the resistivity of silicon wafer is  $3\text{--}5 \Omega\cdot\text{cm}$ . After wet-chemical processes including removal of saw induced damages and texturing, the wafers were cleaned by RCA cleaning procedure. The pyramid size is around  $2\text{--}3 \mu\text{m}$  after texturing. The i<sub>1</sub> layers were deposited by a 13.56 MHz radio frequency (RF) PECVD in the presence of pure silane plasma. The deposition parameters are listed in Table 1. The i<sub>2</sub> layers were deposited under a high H<sub>2</sub> dilution (SiH<sub>4</sub>:H<sub>2</sub>=1:10). The thickness of i<sub>1</sub> and i<sub>2</sub> layer is 4 and 6 nm, respectively. The p/n doped layers with thickness of 10 nm were all deposited by a 40.68MHz very high frequency (VHF) PECVD. The deposition temperature was 200 °C. Tin-doped indium oxide (ITO) films were deposited by sputtering for enhancing the carrier lateral transportation and carrier collection. The device fabrication was finalized by screen printed grid electrodes using silver paste. The device architecture is shown in Fig. 1. Processing details of the SHJ solar cells have been published elsewhere [17–19].

HR-TEM samples were prepared by FEI Helios-600i Nanolab FIB/SEM system, and the thickness of samples is thinned to below 50 nm. Cutting pyramid structure on the rear side of SHJ solar cells along [110] direction. Before cutting samples from cell in the FIB chamber, the electron beam and ion beam were used to deposit the platinum layer on the surface for avoiding the ion beam damage during the sample preparation. The electron beam and ion beam operating at 2 kV and 30 kV, respectively. HR-TEM images were acquired by employing FEI-Titan ETEM, operating at 300kV acceleration voltage.

The microstructure of a-Si:H layer was probed by FTIR (Thermo

Scientific Nicolet iS10). The Current–voltage (I–V) performances of SHJ solar cells were characterized by a triple-A class flash solar simulator under standard test conditions (AM1.5 G, 100 mW/cm<sup>2</sup>, 25 °C). External Quantum efficiency (EQE) measurements were carried out over the spectrum ranges of 300–1180 nm. The minority carrier lifetimes were measured by a Sinton consulting WCT-120 quasi-steady-state photoconductance system in transient mode, and the effective lifetime is determined at an excess carrier density of  $5 \times 10^{15} \text{ cm}^{-3}$ . Structural features of the a-Si:H/c-Si interface were characterized by HR-TEM (FEI Titan ETEM G2).

### 3. Results and discussions

The quality of surface chemical passivation is known to be related to the Si-H bonding states in a-Si:H layer [20]. Microstructure fraction (R) and hydrogen content (C<sub>H</sub>) calculated from FTIR measurement were used to evaluate structural information of a-Si:H films. The FTIR spectra of the i-a-Si:H layers are shown in Fig. 2, fitted with 2 gaussian-distributed absorption peaks centered at wavenumbers of  $2000 \text{ cm}^{-1}$  and  $2090 \text{ cm}^{-1}$ , representing monohydride SiH bond and dihydrides (SiH<sub>2</sub>)<sub>n</sub> bond stretching modes, respectively. The SiH bond is assigned to isolated hydrogen in dense network structure, whereas the (SiH<sub>2</sub>)<sub>n</sub> bond represents clustered hydrogen at the internal surfaces, corresponding to the microscopic voids in the films. The hydrogen content is related to the stretching-mode absorption.

$$C_H = \frac{N_H}{N_H + N_{Si}}$$

$$N_H = A_{2000} + A_{2090}$$

N<sub>Si</sub> is the atomic density of a-Si:H films. N<sub>H</sub> determined from the integrated absorbance of the wagging and stretching modes. Usually,  $A_{2000} = 9 \times 10^{19}$  and  $A_{2090} = 2.2 \times 10^{20} \text{ cm}^{-2}$ , respectively [21].

Microstructure factor R was calculated as follow:  $R = I_{2090}/(I_{2000} + I_{2090})$  [22]. Microstructure factor R and hydrogen content C<sub>H</sub> corresponding to the deposition conditions were listed in Table 1. It is widely accepted that the most important role of hydrogen incorporation is to passivate Si dangling bonds at a-Si:H/c-Si interface [23]. Therefore, a high level hydrogenation at c-Si surface is desired. By tuning the deposition conditions including power density and pressure, we were able to grow a-Si:H films with varied hydrogen content. As shown in Fig. 2, i<sub>1</sub> layers have more (SiH<sub>2</sub>)<sub>n</sub> bonds than i<sub>2</sub> layer, which confirms that i<sub>2</sub> layer has less defects in the film [14]. With increasing deposition rate, the SiH absorption peaks centered at  $2000 \text{ cm}^{-1}$  decreased while (SiH<sub>2</sub>)<sub>n</sub> absorption peaks centered at  $2090 \text{ cm}^{-1}$  increased, indicating hydrogen content C<sub>H</sub> as well as corresponding microstructure factor R was raised from 14.9% to 35.9% and from 4.54% to 74.8%, respectively.

To further investigate the interface morphology, HR-TEM characterization was carried out. Fig. 3(a) and Fig. 3(b) show the cross-

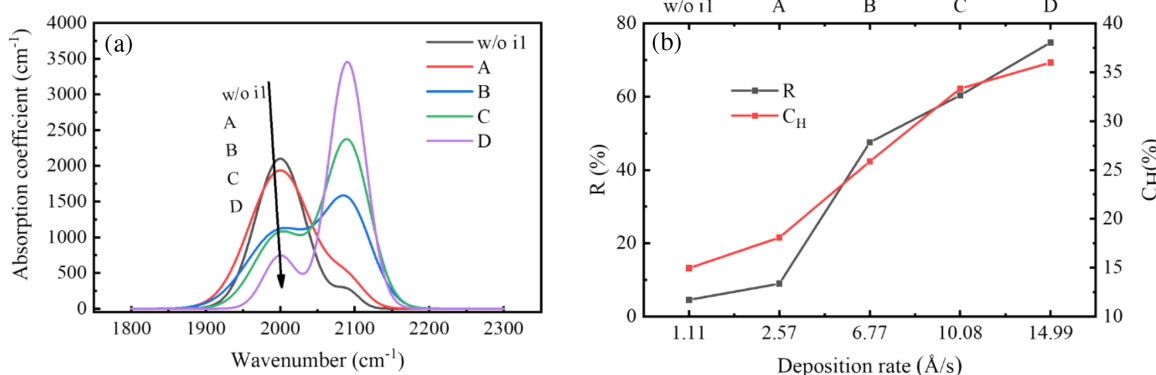
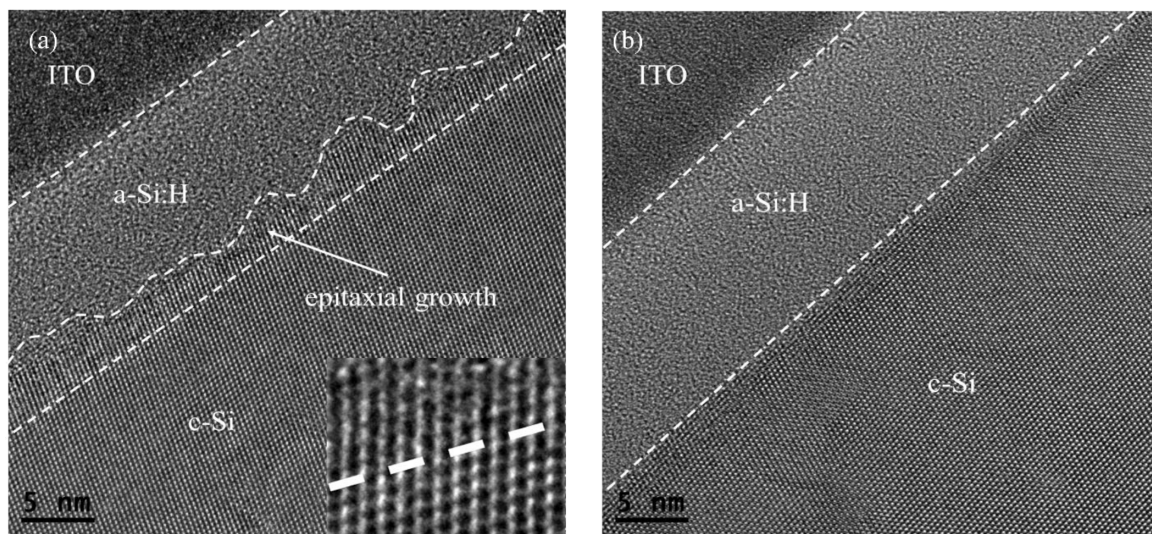


Fig. 2. (a) Infrared absorption spectra of samples deposited at different process conditions (b) The R and CH in a-Si:H films dependency of deposition rate.



**Fig. 3.** HR-TEM images of SHJ solar cells (a) without i<sub>1</sub> buffer layer and the inset was obtained from the box area shows the epitaxial layer structure after magnified (b) with i<sub>1</sub> layer on condition C.

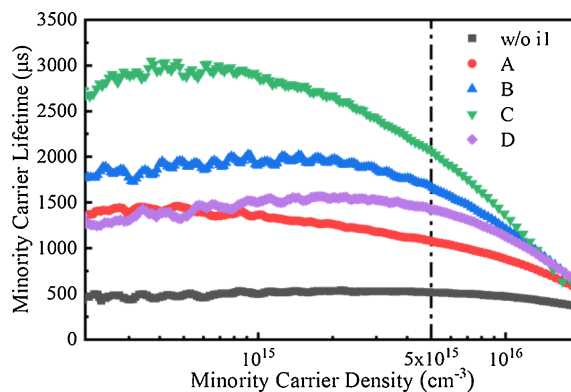
section HR-TEM images of two SHJ solar cells fabricated without and with i<sub>1</sub> layer under condition C, respectively. In both cases, total thickness of the a-Si:H film is nearly 13 nm. In Fig. 3(a) epitaxial growth is clearly observed in the vicinity of a-Si/c-Si interface, which would cause a high density of defects at the c-Si interface [24]. Moreover, it is seen from the inset image of Fig. 3(a) that the lattice structure of epitaxial zone is more disordered than that of the c-Si substrate. On the other hand, as shown in Fig. 3(b), the interface between a-Si:H and c-Si is obviously sharp and clear, and no epitaxial growth is observed at interface.

Fig. 4 shows minority carrier lifetimes of devices with a structure of i-a-Si:H/n-c-Si/i-a-Si:H under different process conditions, which gives direct information of passivation quality at the surface. Minority carrier lifetime of the device without i<sub>1</sub> buffer layer is only 514 μs at an excess carrier density of  $5 \times 10^{15} \text{ cm}^{-3}$ . As long as buffer layer a-Si:H of high hydrogen content was introduced, the minority carrier lifetime increases significantly, indicating that the buffer layer can passivate the surface effectively and thus reduce the surface combination. Many weak-bonding hydrogen atoms will diffuse and saturate interface silicon dangling bonds, reduce defect density at the interface due to the high hydrogen content buffer layer [25, 26]. However, excessive SiH<sub>2</sub> concentration causes too many voids and defects in a-Si:H film as evidenced by decreased minority carrier lifetime in the case of condition D [27]. Therefore, an optimal minority carrier lifetime reaches up to 2050 μs at an excess carrier density of  $5 \times 10^{15} \text{ cm}^{-3}$  under condition C, which is related to less bulk defect density and suppression of epitaxial

growth.

Fig. 5 shows the I-V parameters, including conversion efficiency (Eff), open circuit voltage ( $V_{OC}$ ), short circuit current density ( $J_{SC}$ ), fill factor (FF) and series resistance ( $R_s$ ) under different deposition conditions. Total thickness of the i layer without i<sub>1</sub> buffer layer is the same as that of the cells with buffer layers by increasing thickness of i<sub>2</sub> layer. Conversion efficiencies of the solar cells without i<sub>1</sub> buffer layers are located around 20%, mainly due to low FF and  $V_{OC}$ , which are related to high carrier recombination caused by epitaxial growth at the interface shown in Fig. 3(a). When i<sub>1</sub> buffer layers used, devices performance improved significantly as the FF and  $V_{OC}$  were largely increased. As the  $C_H$  increased from group A to group C, the  $V_{OC}$ , FF and  $J_{SC}$  as well as Eff increased consistently, however when the  $C_H$  further increased as in the case of group D, the  $J_{SC}$  keep increasing slightly while FF dropped dramatically and the  $V_{OC}$  decreased slightly, as a whole resulting in lower Eff to 21%. The reason for the improvement of FF and  $V_{OC}$  is due to suppressed epitaxial growth and improved passivation by increasing the  $C_H$ . While the trend was inverted when  $C_H$  was further increased for group D, which introduced voids and defects into the film to an extent photoconductivity reduction was caused, as indicated by the series resistance ( $R_s$ ) drop in Fig. 5 [28]. Group D with a high hydrogen content leads to a wider bandgap, this affect the carrier transport especially for hole collecting. This is mostly related to band offset, which induce a significant contribution to the  $R_s$  [29]. The change of  $J_{SC}$  will be discussed with QE results separately. The dependency of device performance on  $C_H$  is consistently correlated to the change in minority carrier lifetime. Optimized cell efficiency up to 23.5% was achieved in device group C, with  $V_{OC}$  of 740 mV,  $J_{SC}$  of 38.7 mA/cm<sup>2</sup>, FF of 82%. I-V curves of the solar cell group C and the one without buffer layer were compared in Fig. 6. Efficiency was improved by 3.37% as an absolute value when high  $C_H$  buffer layer was introduced.

The external quantum efficiency (EQE) spectra of SHJ solar cells deposited at various process conditions were plotted as a function of wavelength in Fig. 7. EQE increases significantly in short wavelength with hydrogen content increasing. It is well known that the a-Si:H valence band edge moves down with increasing hydrogen content, leading to a widening of the band gap [30]. From the inset for the transmittance in Fig. 7, less parasitic absorption in short wavelength due to the widening band gap of the a-Si:H film was observed [31]. Therefore, increasing of the integrated  $J_{SC}$  calculated from EQE from 40.2 to 40.6 mA/cm<sup>2</sup> is ascribed to wider bandgap of i<sub>1</sub> layer with higher  $C_H$ , which is consistent with the  $J_{SC}$  gain in I-V measurements. The difference on the range 1000-1200 may causes by ITO films, a little water vapor will



**Fig. 4.** Minority carrier lifetimes of devices processed under different conditions.

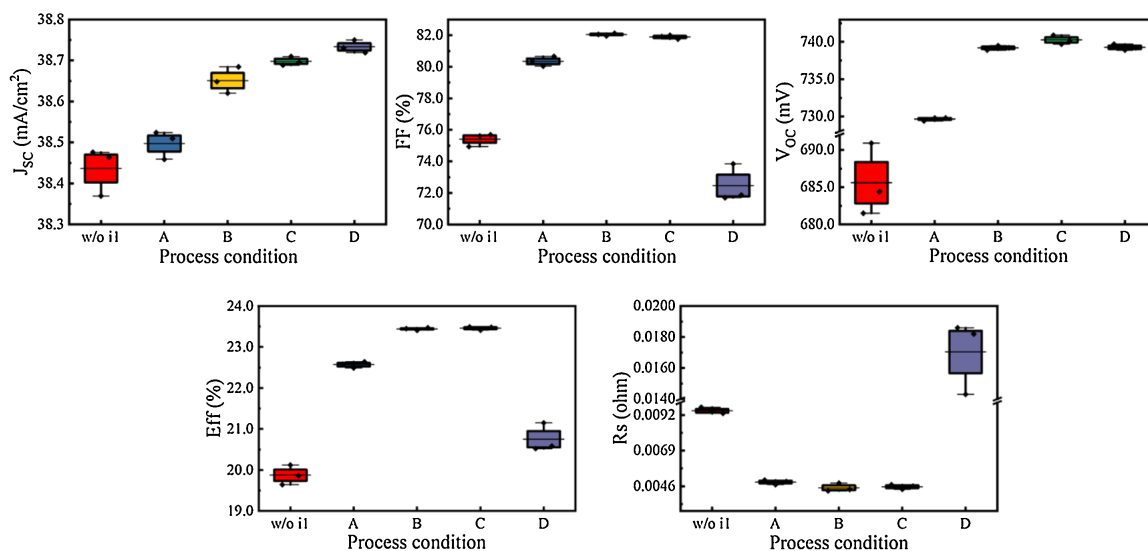


Fig. 5. I-V parameters of SHJ solar cells processed under varied conditions.

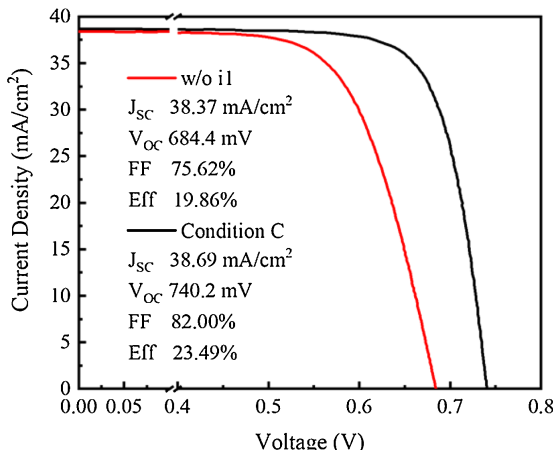


Fig. 6. I-V curves of SHJ solar cells deposited without  $i_1$  buffer layer and under condition C.

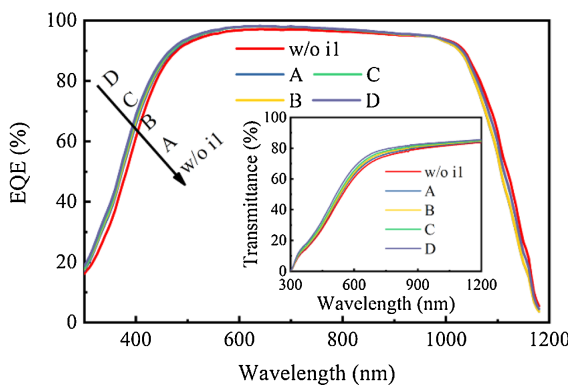


Fig. 7. The EQE of SHJ solar cells with different  $i$  layers. The inset shows the transmittance of a-Si:H film with different  $i$  layers.

influence the IR part of EQE spectrum [32], it's difficult to be controlled in industrial production line.

Compared with other research groups [33–37], our cells have a high  $V_{OC}$  and a quite good FF. However, the  $J_{SC}$  is much lower than others. We further optimized the  $J_{SC}$  by using a n-μc-Si window layer which improved the  $J_{SC}$  effectively [38].

#### 4. Conclusion

In this study, a high  $C_H$  buffer layer  $i_1$  was introduced between bulk a-Si:H layer and c-Si surface, which effectively passivated the surface and thus significantly improved the conversion efficiency of SHJ solar cells. HR-TEM characterization shows that clear interface was formed and no epitaxial growth was involved when buffer layer was deposited prior to bulk  $i_2$  layer. It was found that the device performance was correlated to hydrogen content  $C_H$  of the buffer layer, which was determined by varied processing conditions and calibrated from FTIR spectra. As hydrogen content increases,  $V_{OC}$ , FF and  $J_{SC}$  as well as efficiency of the SHJ solar cells were greatly improved in the presence of buffer layer, yet too much hydrogen might introduce defects to an extent that would lead to bad device performance. As a result, our champion cell with this powerful passivation buffer layer is at a high level of 23.5%, with  $V_{OC}$  of 740 mV,  $J_{SC}$  of 38.7 mA/cm<sup>2</sup>, FF of 82% was achieved on M2 wafer (total area 242.5 cm<sup>2</sup>).

#### CRediT author statement

**Tianyu Ruan:** Methodology, Investigation, Data Curation, Writing - Original Draft **Minghao Qu:** Conceptualization, Supervision, Writing-Review & Editing **Xianlin Qu:** Resources, Data Curation **Xiaoning Ru:** Validation, Investigation **Jianqiang Wang:** Investigation **Yongcai He:** Investigation **Kun Zheng:** Funding acquisition, Resources **Bo He:** Writing - Review & Editing **Hongfeng Lin :** Writing - Review & Editing **Xixiang Xu:** Project administration **Yongzhe Zhang:** Funding acquisition, Writing - Review & Editing **Hui Yan:** Project administration, Funding acquisition, Writing - Review & Editing

#### Declaration of Competing interest

The authors declare that they have no known competing financial interests or personal relationships that could have appeared to influence the work reported in this paper.

#### Acknowledgment

This work was supported by the National Natural Science Foundation of China (61974008, 61922005, 11774016) and the National Key Research and Development Program of China (grant number 2016YFB0700703).

Authors would thank Min Peng, Yan Zeng, Gangqiang Dong, and Shi

Yin for sample preparation, cell fabrication, and characterization. Supports from Kaiwang Zhang, Na Yang, and Zheng Ma in equipment and facility maintenance are greatly appreciated.

## Reference

- [1] K. Yoshikawa, W. Yoshida, T. Irie, H. Kawasaki, K. Konishi, H. Ishibashi, T. Asatani, D. Adachi, M. Kanematsu, H. Uzu, K. Yamamoto, Exceeding conversion efficiency of 26% by heterojunction interdigitated back contact solar cell with thin film Si technology, *Sol. Energy Mater. Sol. Cells* 173 (2017) 37–42, <https://doi.org/10.1016/j.solmat.2017.06.024>.
- [2] M.A. Green, The path to 25% silicon solar cell efficiency: history of silicon cell evolution, *Prog. Photovoltaics Res. Appl.* 17 (2009) 183–189, <https://doi.org/10.1002/pip.892>.
- [3] D. Adachi, J.L. Hernández, K. Yamamoto, Impact of carrier recombination on fill factor for large area heterojunction crystalline silicon solar cell with 25.1% efficiency, *Appl. Phys. Lett.* 107 (2015) 233506, , <https://doi.org/10.1063/1.4937224>.
- [4] C. Hollermann, F. Haase, S. Schäfer, J. Krieger, R. Brendel, R. Peibst, 26.1%-efficient POLO-IBC cells: quantification of electrical and optical loss mechanisms, *Prog. Photovoltaics Res. Appl.* 27 (2019) 950–958, <https://doi.org/10.1002/pip.3098>.
- [5] A. Descoedres, J. Horzel, B. Paviet-Salomon, L.-L. Senaud, G. Christmann, J. Geissbühler, P. Wyss, N. Badel, J.-W. Schütttauf, J. Zhao, C. Allebé, A. Faes, S. Nicolay, C. Ballif, M. Despeisse, The versatility of passivating carrier-selective silicon thin films for diverse high-efficiency screen-printed heterojunction-based solar cells, *Prog. Photovoltaics Res. Appl.* (2019), <https://doi.org/10.1002/pip.3227>.
- [6] D. Lachenal, P. Papet, B. Legradic, R. Kramer, T. Kössler, L. Andreetta, N. Holm, W. Frammersberger, D.L. Baetzner, B. Strahm, L.L. Senaud, J.W. Schütttauf, A. Descoedres, G. Christmann, S. Nicolay, M. Despeisse, B. Paviet-Salomon, C. Ballif, Optimization of tunnel-junction IBC solar cells based on a series resistance model, *Sol. Energy Mater. Sol. Cells* 200 (2019) 110036, , <https://doi.org/10.1016/j.solmat.2019.110036>.
- [7] A. Descoedres, C. Allebé, N. Badel, L. Barraud, J. Champliaud, G. Christmann, F. Debrot, A. Faes, J. Geissbühler, J. Horzel, A. Lachowicz, J. Levrat, S. Martin de Nicolas, S. Nicolay, B. Paviet-Salomon, L.L. Senaud, C. Ballif, M. Despeisse, Low-temperature processes for passivation and metallization of high-efficiency crystalline silicon solar cells, *Solar Energy* 175 (2018) 54–59, <https://doi.org/10.1016/j.solener.2018.01.074>.
- [8] J. Haschke, O. Dupré, M. Boccard, C. Ballif, Silicon heterojunction solar cells: recent technological development and practical aspects - from lab to industry, *Sol. Energy Mater. Sol. Cells* 187 (2018) 140–153, <https://doi.org/10.1016/j.solmat.2018.07.018>.
- [9] M. Taguchi, A. Terakawa, E. Maruyama, M. Tanaka, Obtaining a higher voc in HIT cells, *Prog. Photovoltaics Res. Appl.* 13 (2005) 481–488, <https://doi.org/10.1002/pip.646>.
- [10] J. Schmidt, R. Peibst, R. Brendel, Surface passivation of crystalline silicon solar cells: present and future, *Sol. Energy Mater. Sol. Cells* 187 (2018) 39–54, <https://doi.org/10.1016/j.solmat.2018.06.047>.
- [11] S. Olibet, E. Vallat-Sauvain, C. Ballif, Model for a-Si: h/c-Si interface recombination based on the amphoteric nature of silicon dangling bonds, *Physical Review B* 76 (2007) 035326, , <https://doi.org/10.1103/PhysRevB.76.035326>.
- [12] Y. Zhang, C. Yu, M. Yang, L.-R. Zhang, Y.-C. He, J.-Y. Zhang, X.-X. Xu, Y.-Z. Zhang, X.-M. Song, H. Yan, Significant Improvement of Passivation Performance by Two-Step Preparation of Amorphous Silicon Passivation Layers in Silicon Heterojunction Solar Cells, *Chinese Physics Letters* 34 (2017) 038101, , <https://doi.org/10.1088/0256-307X/34/3/038101>.
- [13] W. Liu, L. Zhang, R. Chen, F. Meng, W. Guo, J. Bao, Z. Liu, Underdense a-Si:h film capped by a dense film as the passivation layer of a silicon heterojunction solar cell, *J. Appl. Phys.* 120 (2016) 175301, , <https://doi.org/10.1063/1.4966941>.
- [14] J.C. Knights, G. Lucovsky, R.J. Nemanich, Defects in plasma-deposited a-Si: H, *J. Non-Cryst. Solids* 32 (1979) 393–403, [https://doi.org/10.1016/0022-3093\(79\)90084-X](https://doi.org/10.1016/0022-3093(79)90084-X).
- [15] M. Mews, T.F. Schulze, N. Mingirulli, L. Korte, Hydrogen plasma treatments for passivation of amorphous-crystalline silicon-heterojunctions on surfaces promoting epitaxy, *Appl. Phys. Lett.* 102 (2013) 122106, , <https://doi.org/10.1063/1.4798292>.
- [16] W. Liu, L. Zhang, R. Chen, F. Meng, W. Guo, J. Bao, Z. Liu, Underdense a-Si: h film capped by a dense film as the passivation layer of a silicon heterojunction solar cell, *J. Appl. Phys.* 120 (2016) 175301, , <https://doi.org/10.1063/1.4966941>.
- [17] C. Yu, M. Yang, G. Dong, F. Peng, D.-C. Hu, W. Long, C. Hong, G. Cui, J. Wang, Y. He, H. Yan, J. Zhang, Y. Li, X. Xu, Development of silicon heterojunction solar cell technology for manufacturing, *Jpn. J. Appl. Phys.* 57 (2018) 08RB15, <https://doi.org/10.7567/jjap.57.08rb15>.
- [18] Y. Zhang, C. Yu, M. Yang, Y. He, L. Zhang, J. Zhang, X. Xu, Y. Zhang, X. Song, H. Yan, Optimization of the window layer in large area silicon heterojunction solar cells, *RSC advances* 7 (2017) 9258–9263.
- [19] T. Ruan, M. Qu, J. Wang, Y. He, X. Xu, C. Yu, Y. Zhang, H. Yan, Effect of deposition temperature of a-Si:h layer on the performance of silicon heterojunction solar cell, *Journal of Materials Science: Materials in Electronics* 30 (2019) 13330–13335, <https://doi.org/10.1007/s10854-019-01700-7>.
- [20] D. Han, K. Wang, J.M. Owens, L. Gedvilas, B. Nelson, H. Habuchi, M. Tanaka, Hydrogen structures and the optoelectronic properties in transition films from amorphous to microcrystalline silicon prepared by hot-wire chemical vapor deposition, *J. Appl. Phys.* 93 (2003) 3776–3783, <https://doi.org/10.1063/1.1555680>.
- [21] A.A. Langford, M.L. Fleet, B.P. Nelson, W.A. Lanford, N. Maley, Infrared absorption strength and hydrogen content of hydrogenated amorphous silicon, *Physical Review B* 45 (1992) 13367, <https://doi.org/10.1103/PhysRevB.45.13367>.
- [22] E. Bhattacharya, A.H. Mahan, Microstructure and the light-induced metastability in hydrogenated amorphous silicon, *Appl. Phys. Lett.* 52 (1988) 1587–1589, <https://doi.org/10.1063/1.99089>.
- [23] W.G.J.H.M. van Sark, L. Korte, F. Roca, *Physics and Technology of Amorphous-Crystalline Heterostructure Silicon Solar Cells*, Springer Berlin Heidelberg, Berlin, Heidelberg, 2012.
- [24] H. Fujiwara, T. Kaneko, M. Kondo, Application of hydrogenated amorphous silicon oxide layers to c-Si heterojunction solar cells, *Appl. Phys. Lett.* 91 (2007) 133508, , <https://doi.org/10.1063/1.2790815>.
- [25] T.F. Schulze, H.N. Beushausen, T. Hansmann, L. Korte, B. Rech, Accelerated interface defect removal in amorphous/crystalline silicon heterostructures using pulsed annealing and microwave heating, *Appl. Phys. Lett.* 95 (2009) 182108, , <https://doi.org/10.1063/1.3255018>.
- [26] A. Descoedres, L. Barraud, S. De Wolf, B. Strahm, D. Lachenal, C. Guérin, Z.C. Holman, F. Zicarelli, B. Demaurex, J. Seif, Improved amorphous/crystalline silicon interface passivation by hydrogen plasma treatment, *Appl. Phys. Lett.* 99 (2011) 123506, , <https://doi.org/10.1063/1.3641899>.
- [27] W. Guo, L. Zhang, F. Meng, J. Bao, D. Wang, J. Liu, Z. Feng, P.J. Vierlinden, Z. Liu, Study of the correlation between hydrogenated amorphous silicon microstructure and crystalline silicon surface passivation in heterojunction solar cells, *physica status solidi (a)* 212 (2015) 2233–2238, <https://doi.org/10.1002/pssa.201532143>.
- [28] M. Isomura, M. Kondo, A. Matsuda, Device-grade amorphous silicon prepared by high-pressure plasma, *Jpn. J. Appl. Phys.* 41 (2002) 1947.
- [29] J.P. Seif, D. Menda, A. Descoedres, L. Barraud, O. Özdemir, C. Ballif, S. De Wolf, Asymmetric band offsets in silicon heterojunction solar cells: impact on device performance, *J. Appl. Phys.* 120 (2016) 054501, , <https://doi.org/10.1063/1.4959988>.
- [30] T.F. Schulze, L. Korte, F. Ruske, B. Rech, Band lineup in amorphous/crystalline silicon heterojunctions and the impact of hydrogen microstructure and topological disorder, *Physical Review B* 83 (2011) 165314, , <https://doi.org/10.1103/PhysRevB.83.165314>.
- [31] Z.C. Holman, A. Descoedres, L. Barraud, F.Z. Fernandez, J.P. Seif, S. De Wolf, C. Ballif, Current losses at the front of silicon heterojunction solar cells, *IEEE Journal of Photovoltaics* 2 (2012) 7–15.
- [32] L. Barraud, Z.C. Holman, N. Badel, P. Reiss, A. Descoedres, C. Battaglia, S. De Wolf, C. Ballif, Hydrogen-doped indium oxide/indium tin oxide bilayers for high-efficiency silicon heterojunction solar cells, *Sol. Energy Mater. Sol. Cells* 115 (2013) 151–156, <https://doi.org/10.1016/j.solmat.2013.03.024>.
- [33] J. Zhao, M. Konig, Y. Yao, Y. Wang, R. Zhou, T. Xie, H. Deng, >24% Silicon Heterojunction Solar Cells on Meyer Burger's on Mass Production Tools and How Wafer Material Impacts Cell Parameters, 2018 IEEE 17th World conference on photovoltaic energy conversion, 201818288312, , <https://doi.org/10.1109/PVSC.2018.8547908>.
- [34] M. Taguchi, A. Yano, S. Tohoda, K. Matsuyama, Y. Nakamura, T. Nishiwaki, K. Fujita, E. Maruyama, 24.7% Record Efficiency HIT Solar Cell on Thin Silicon Wafer, *IEEE J. Photovoltaics* 4 (2014) 96–99, <https://doi.org/10.1109/JPHOTOV.2013.2282737>.
- [35] D. Adachi, J.L. Hernandez, K. Yamamoto, Impact of carrier recombination on fill factor for large area heterojunction crystalline silicon solar cell with 25.1% efficiency, *Appl. Phys. Lett.* 107 (2015) 233506, , <https://doi.org/10.1063/1.4937224>.
- [36] Z. Wu, L. Zhang, R. Chen, W. Liu, Z. Li, F. Meng, Z. Liu, Improved amorphous/crystalline silicon interface passivation for silicon heterojunction solar cells by hot-wire atomic hydrogen during doped a-Si:h deposition, *Appl. Surf. Sci.* 475 (2019) 504–509, <https://doi.org/10.1016/j.apsusc.2018.12.239>.
- [37] A.N. Fioretti, M. Boccard, R. Monnard, C. Ballif, Low-Temperature p-Type Microcrystalline Silicon as Carrier Selective Contact for Silicon Heterojunction Solar Cells, *IEEE J. Photovoltaics* 9 (2019) 1158–1165, <https://doi.org/10.1109/JPHOTOV.2019.2917550>.
- [38] C. Lei, C. Peng, J. Zhong, H. Li, M. Yang, K. Zheng, X. Qu, L. Wu, C. Yu, Y. Li, Phosphorus treatment to promote crystallinity of the microcrystalline silicon front contact layers for highly efficient heterojunction solar cells, *Sol. Energy Mater. Sol. Cells* 209 (2020) 110439, , <https://doi.org/10.1016/j.solmat.2020.110439>.